RESEARCH ARTICLE

DGD Development, Growth & Differentiation   WILEY

Pcgf1 gene disruption reveals primary involvement of epigenetic mechanism in neuronal subtype specification in the enteric nervous system

Bayu Pratama Putra[1] | Keisuke Ito[1] | Carla Cirillo[1,2] | Mukhamad Sunardi[1] | Haruhiko Koseki[3] | Toshihiro Uesaka[1] | Hideki Enomoto[1]

[1]Division of Neural Differentiation and Regeneration, Department of Physiology and Cell Biology, Kobe University Graduate School of Medicine, Kobe, Japan

[2]Toulouse NeuroImaging Center (ToNIC), Inserm, University of Toulouse-Paul Sabatier, Toulouse, France

[3]Laboratory for Developmental Genetics, RIKEN Center for Integrative Medical Sciences, Yokohama, Japan

Correspondence
Hideki Enomoto, Division of Neural Differentiation and Regeneration, Department of Physiology and Cell Biology, Kobe University Graduate School of Medicine, Kobe, Japan.
Email: enomotoh@med.kobe-u.ac.jp

Abstract

The enteric nervous system (ENS) regulates gut functions independently from the central nervous system (CNS) by its highly autonomic neural circuit that integrates diverse neuronal subtypes. Although several transcription factors are shown to be necessary for the generation of some enteric neuron subtypes, the mechanisms underlying neuronal subtype specification in the ENS remain elusive. In this study, we examined the biological function of Polycomb group RING finger protein 1 (PCGF1), one of the epigenetic modifiers, in the development and differentiation of the ENS by disrupting the *Pcgf1* gene selectively in the autonomic-lineage cells. Although ENS precursor migration and enteric neurogenesis were largely unaffected, neuronal differentiation was impaired in the *Pcgf1*-deficient mice, with the numbers of neurons expressing somatostatin (Sst^+) decreased in multiple gut regions. Notably, the decrease in Sst^+ neurons was associated with the corresponding increase in $calbindin^+$ neurons in the proximal colon. These findings suggest that neuronal subtype conversion may occur in the absence of PCGF1, and that epigenetic mechanism is primarily involved in specification of some enteric neuron subtypes.

KEYWORDS

enteric nervous system, epigenetic mechanism, neuronal subtype conversion, neuronal subtype specification, PCGF1

1 | INTRODUCTION

The enteric nervous system (ENS) is often called "the second brain" based on its ability to regulate motility, secretion, and blood flow of the gut without inputs from the central nervous system (CNS) (Avetisyan et al., 2015). Such independent functions of the ENS are made possible by its autonomic neural circuit residing in the gut wall, in which various neuronal subtypes are functionally integrated (Hao et al., 2016; Hao & Young, 2009). At least 12 neuronal subtypes are present in the ENS

(Morarach et al., 2021). Although each neuronal subtype has its differentiation timeline, varying from as early as embryonic day (E) 8 to postnatal periods (Bergner et al., 2014; Marlene M. Hao & Young, 2009), the molecular mechanism underlying the generation of neuronal diversity in the ENS remains largely unknown. In the CNS, the fate of a given neuronal subtype is determined by the actions of specific transcription factors induced by the concentration gradient of bone morphogenetic proteins (BMPs) and sonic hedgehog (Shh) in the neural tube (Molyneaux et al., 2007). Transcriptional control of neuronal

subtype specification was also demonstrated in the ENS by several mouse studies, in which genetic disruption of transcription factors, *Pbx3*, *Sox6*, and *Tbx3* showed impaired differentiation of some enteric neuronal subtypes (Memic et al., 2018; Morarach et al., 2021; Wright et al., 2021). However, overall mechanisms underlying neuronal subtype specification in the ENS have yet to be elucidated.

Polycomb group proteins are the epigenetic modifiers that regulate cell differentiation via chromatin compaction and modification (Yan et al., 2017). They are grouped into two multiprotein complexes, Polycomb repressive complexes 1 and 2 (PRC1 and PRC2), which consist of the specific core subunits, and can epigenetically silence gene transcription via histone modifications (Aranda et al., 2015; Fursova et al., 2019). In cell lineage determination, it is generally accepted that transcription factors activate or silence gene expression, thereby determining the cell fate, and epigenetic mechanisms successively stabilize the gene expression status. A recent study showed that disruption of the components of the PRC1 complex led to cell fate conversion in the hematopoietic lineage (Ikawa et al., 2016), demonstrating that the epigenetic mechanism can primarily regulate cell fate determination.

Both PRC1 and PRC2 are involved in several neurodevelopmental events in a spatiotemporal manner (Feng & Sun, 2022; Fukuda et al., 2011; Kim et al., 2011; Kim et al., 2018). Polycomb group RING finger protein 1 (PCGF1), a member of the PRC1, also known as Nervous System Polycomb-1 (NSPC1), is involved in the neural induction stage, stem cell renewal, and differentiation (Li et al., 2021; Yan et al., 2017). During mid-gestation, *Pcgf1* is highly expressed in the peripheral nervous system, including the dorsal root ganglion, sympathetic and parasympathetic ganglia, and ENS (Morarach et al., 2021; Nunes et al., 2001; Vohra et al., 2006). The PCGF1–PRC1 complex is essential to shape Polycomb chromatin domains and initiate gene repression during differentiation along with PRC2 recruitment (Blackledge et al., 2014; Fursova et al., 2019; Sugishita et al., 2021).

In this study, we examined the biological function of PCGF1 in the development and maturation of the ENS using a $Pcgf1^{fl/fl}$; $Phox2b^{Cre/+}$ mice, in which *Pcgf1* was selectively ablated in cells of the autonomic lineage. We provide evidence on the possible epigenetic regulation of neuronal subtype specification in the ENS.

2 | MATERIALS AND METHODS

2.1 | Animals

$Pcgf1^{fl/+}$ (RBRC11692, RIKEN BioResource Research Center, Japan) (Almeida et al., 2017) and $Phox2b^{Cre/+}$ mice (generated as described in Data S1 and Figure S1a–e) were maintained on the C57BL/6N background. The *Pcgf1* conditional knockout (cKO) mice were generated by crossing *Pcgf1* floxed mice with $Phox2b^{Cre/+}$ mice ($Pcgf1^{fl/fl}$; $Phox2b^{Cre/+}$). The study was approved by the Institutional Animal Care and Use Committee, in line with implementing Kobe University Animal Experimentation Regulations. All the experiments were performed following the ARRIVE guidelines (Kilkenny et al., 2010) and carried out in accordance

with Kobe University's guide for the care and use of laboratory animals. Mice were kept in specific pathogen-free (SPF) conditions in plastic cages (CL-0123-3, CLEA Japan, Tokyo, Japan) with animal bedding (white flake, 9201100, Jackson Laboratory, Japan) at 25°C with a 12 hr light/12 hr dark cycle. The mice were fed ad libitum of food (normal diet DC-8, 23.1% crude protein, and 3,590 kcal/kg, CLEA Japan, Tokyo, Japan) and water. Mice of either sex were used for each experiment in this study. Mice were euthanized as a humane endpoint if young mice failed to gain weight relative to wild-type (WT) control and were unable to stand.

2.2 | Gastrointestinal transit time and fecal water content

Total gastrointestinal transit time (GITT) was examined according to a previous report (Sunardi et al., 2022). Mice (3 weeks old) were individually separated in a non-food cage and gavaged with 10 μL/body weight (in grams) of the prepared solution of 6% carmine red dye (Sigma-Aldrich, MO, USA) dissolved in 0.5% methylcellulose (Sigma-Aldrich, MO, USA). The transit time (in minutes) was determined based on the excretion of the first fecal pellet tainted with carmine red. Determination of water content in feces was performed as previously described (Vicentini et al., 2021). Briefly, fecal pellets were collected every 15 min over 1 hr, then counted and weighed as a wet pellet. Fecal pellets were placed at 50°C for 24 hr, and the dry pellet's weight was determined. Fecal water contents (in %) were calculated as follows: (wet pellet − dry pellet)/wet pellet × 100%.

2.3 | In situ hybridization

Based on previous study (Yoshioka et al., 2022), in situ hybridization (ISH) was performed on a 16 μm section of E13.5 embryos. *Pcgf1* digoxigenin (DIG)-labeled cRNA probe was synthesized from a DNA fragment of the *Pcgf1* cDNA (nucleotide 33–382) using the DIG RNA Labeling Kit (11175025910, Roche, Basel, Switzerland). The riboprobe was detected by using an anti-DIG antibody conjugated with alkaline phosphatase (1:2,000 dilution, 11207733910, Roche, Basel, Switzerland), and the signal developed using 5-bromo-4-chloro-3-indolyl phosphate (ThermoFisher, MA, USA) and nitro blue tetrazolium (ThermoFisher, MA, USA) as color substrate. Representative images were captured by the Keyence HS All-in-one fluorescence microscope BZ-9000 (Keyence, Osaka, Japan).

2.4 | Immunohistochemistry

Embryonic gut was dissected from E14.5 embryos and P0 neonatal mice for whole-mount immunohistochemistry (IHC). Collected gut tissue was fixed with 4% paraformaldehyde (PFA) overnight at 4°C. After fixation, the gut was washed with 0.1% Triton X-100/phosphate-buffered saline (PBS) for 3 × 30 min and

TABLE 1 List of primary and secondary antibodies used in the study.

	Dilution	Source	Catalog number	RRID
Primary antibodies				
Rabbit anti-UCHL1/PGP9.5	1:500	Proteintech	14730-1-AP	AB_2210497
Guinea pig anti-Phox2B	1:500	(Sunardi et al., 2022)		AB_2895590
Rabbit anti-HuD + HuC	1:500	Abcam	AB184267	AB_2864321
Rabbit anti-calretinin	1:500	Merck	SAB5600135	AB_2934263
Rabbit anti-NOS1	1:500	Merck	AB5380	AB_91824
Rabbit anti-somatostatin	1:500	GeneTex	GTX133119	AB_2814698
Rabbit anti-calbindin	1:500	Abcam	AB108404	AB_10861236
Secondary antibodies				
Alexa Fluor Plus 488 donkey anti-rabbit IgG	1:1,000	Thermo Fisher	A32790	AB_2762833
CF568 donkey anti-rabbit IgG	1:500	Biotium	20098	AB_10557118
CF568 donkey anti-guinea pig IgG	1:500	Biotium	20377	AB_2934264

blocked by a blocking buffer containing 5% dimethyl sulfoxide (DMSO), 5% skim milk, and 1% Tween-20 in PBS for 1 hr at room temperature (RT). Samples were incubated with primary antibodies diluted in the blocking buffer overnight at 4°C. The following day, samples were washed with permeabilizing buffer (5% DMSO and 1% Tween-20 in PBS) for 3×30 min, and appropriate secondary antibodies were applied overnight at 4°C. The samples were then washed with permeabilizing buffer and mounted with 50% glycerol in PBS.

For analyses of 3-week-old mice, duodenum, jejunum, ileum, proximal, and distal colon were collected, and the myenteric and submucosal preparations were obtained (Chalazonitis et al., 2001). Tissues were fixed in 4% PFA overnight at 4°C. The myenteric preparations were blocked in a blocking buffer containing 0.5% Triton X-100/PBS with donkey serum for 2 hr at RT. The submucosal preparations were first incubated in 100% DMSO for 30 min at RT for cell permeabilization and then in blocking buffer containing 1% bovine serum albumin (BSA), 0.3% Triton X-100, and 0.2% skim milk in PBS for 1 hr at RT. Primary antibodies in the blocking buffer were then applied overnight at 4°C. Samples were washed and incubated with appropriate secondary antibodies for 2 hr at RT. Samples were then washed and mounted using 50% glycerol in PBS. Primary and secondary antibodies used for the IHC procedure are listed in Table 1.

2.5 | Cell counting and imaging

Cell counting was done in 3-week-old mouse tissue based on specific antibody-positive ($^+$) cells in the myenteric and submucosal plexus from the duodenum, jejunum, ileum, proximal, and distal colon. By selecting 10 random view fields at 20× magnification (1.13 mm^2), cell numbers were counted using Zeiss Axioskop 2 Plus microscope (Zeiss, Jena, Germany). For quantification in E14.5 and P0 mice gut, five random view fields on 10× magnification (0.4 mm^2) were selected, and Phox2B$^+$ neurons were counted using ImageJ software (Schneider et al., 2012) (Phox2b$^{Cre/+}$ [$n = 5$], Pcgf1$^{fl/fl}$; Phox2b$^{Cre/+}$

[$n = 4$]). Representative images were captured by the Zeiss LSM 900 confocal microscope (Zeiss, Jena, Germany). Images were adjusted for contrast and brightness before overlay and quantification using ImageJ software (Schneider et al., 2012).

2.6 | BaseScope ISH assay and IHC

We performed the BaseScope ISH Assay using the BaseScope™ Reagent Kit v2-RED (323900, Advanced Cell Diagnostics, NJ, USA) to detect Pcgf1 RNA expression by Pcgf1-specific probe (1199581-C1, Advanced Cell Diagnostics, NJ, USA) in the ENS of 3-week-old mouse tissue. Briefly, the myenteric preparations from the proximal colon of WT and Pcgf1$^{fl/fl}$; Phox2b$^{Cre/+}$ mice were incubated with 50%, 70%, and 100% ethanol, respectively, for 5 min. Protease treatment was then performed in all samples for 45 min at RT, followed by 5×10 min of washing at RT with wash buffer. Pcgf1 probe was then applied overnight at 40°C. Samples were then incubated with AMP1 to AMP8 kit reagents, followed by BaseScope™ Fast RED A and B incubation, according to the manufacturer's protocol. Immunofluorescent counterstaining was then performed using a HuC/D primary antibody (Table 1).

2.7 | Statistical analysis

GraphPad Prism 8 software (GraphPad Software, CA, USA) was used for statistical analysis. The data are shown as mean ± standard error of the mean (SEM). The Shapiro–Wilk normality test was conducted to determine whether the data followed a Gaussian distribution. We used the unpaired t-test with Welch's correction test for body weight, GITT, and fecal water contents for normal distribution data. The Mann–Whitney U test was used to analyze non-normal data for myenteric and submucosal plexus neuron numbers. The Kaplan–Meier method was used for survival analysis data and analyzed by the log-rank test. We used a cutoff of $p < 0.05$ as statistically significant data in each quantitative figure.

3 | RESULTS

Pcgf1-deficient mice die in early development (E9.5) due to various morphological defects (Sugishita et al., 2021), and the biological role of PCGF1 in the later developmental periods remains largely elusive. To understand the role of PCGF1 in ENS development, we utilized the *Pcgf1*-floxed allele (Almeida et al., 2017) and planned to disrupt the *Pcgf1* gene in the early ENS development via Cre-lox recombination. To this end, we generated *Phox2b*-Cre knock-in mice by gene targeting followed by genome editing (Figure S1a–e). In the developing peripheral nervous system, *Phox2b* is expressed immediately after the specification of the autonomic lineage, including the enteric, sympathetic, and parasympathetic ganglia (Nunes et al., 2001). We crossed *Pcgf1*-floxed mice to *Phox2b*$^{Cre/+}$ mice and obtained *Pcgf1*$^{fl/fl}$; *Phox2b*$^{Cre/+}$ mice. To confirm whether the *Pcgf1* gene was

successfully disrupted in the autonomic lineage of these mice, we conducted ISH analysis on E13.5 embryos using riboprobes that hybridize the floxed genomic region of the *Pcgf1* gene. This analysis revealed the absence of *Pcgf1* expression in the ENS and the sympathetic chain but not in the dorsal root ganglion (DRG) in *Pcgf1*$^{fl/fl}$; *Phox2b*$^{Cre/+}$ embryos, confirming the disruption of the *Pcgf1* gene in the autonomic nervous system (Figure 1a). In the postnatal ENS, *Pcgf1* is almost ubiquitously expressed in enteric neurons. We also validated the absence of *Pcgf1* transcripts in the myenteric plexus of *Pcgf1*$^{fl/fl}$; *Phox2b*$^{Cre/+}$ mice (3 weeks old), as shown by the BaseScope in situ assay (Figure 1b).

Pcgf1$^{fl/fl}$; *Phox2b*$^{Cre/+}$ mice displayed small body size at the postnatal stage of 3 weeks old (Figure 2a). We, therefore, compared growth and mortality rates among *Pcgf1*$^{fl/fl}$; *Phox2b*$^{Cre/+}$, WT, and *Phox2b*$^{Cre/+}$ mice. Although both WT and *Phox2b*$^{Cre/+}$ had similar
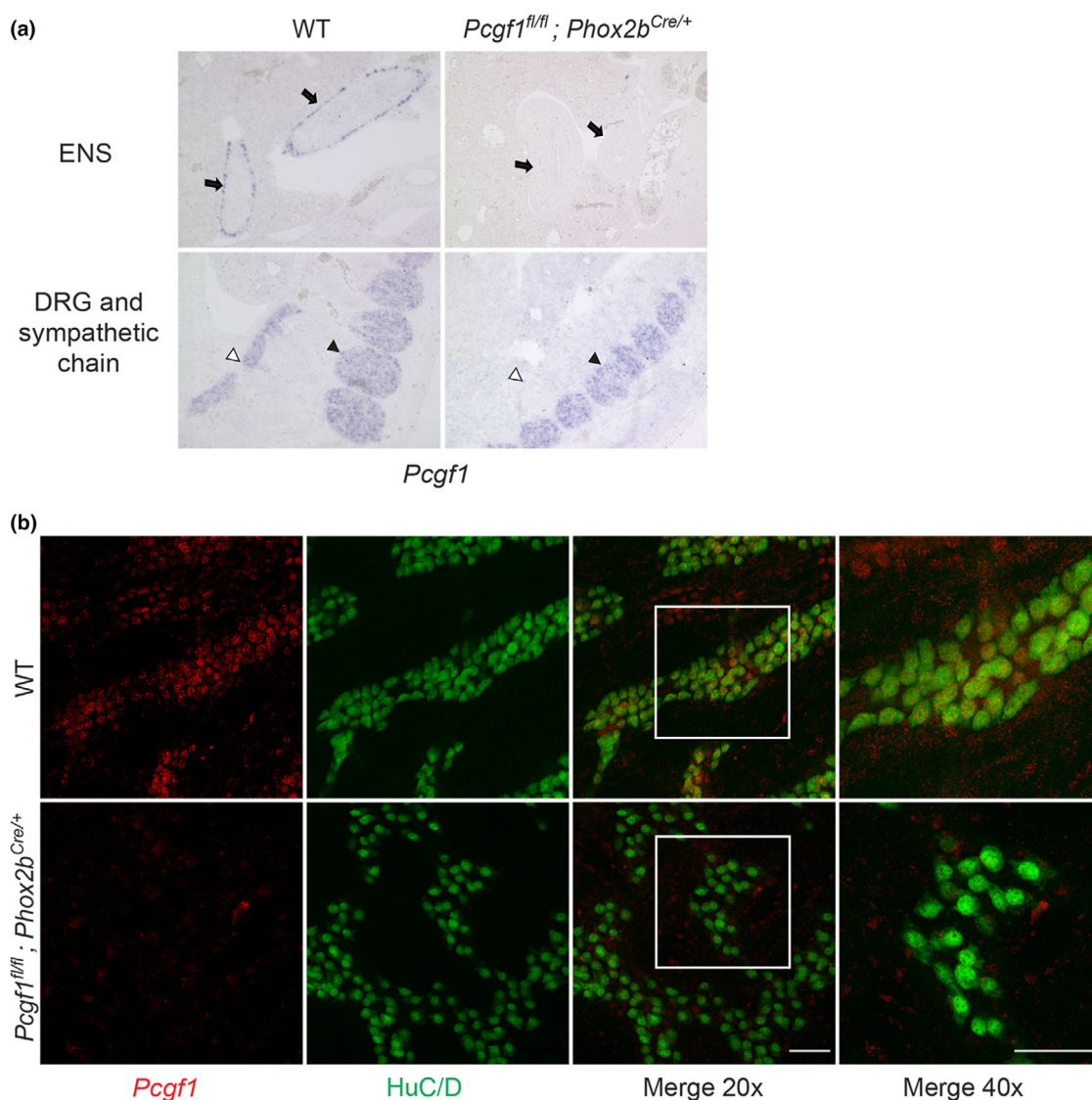
FIGURE 1 Expression and selective deletion of *Pcgf1* in the autonomic nervous system. (a) In situ hybridization (ISH) on E13.5 WT and *Pcgf1*$^{fl/fl}$; *Phox2b*$^{Cre/+}$ embryos by analysis using *Pcgf1* probe. Arrows show the ENS, white and black arrowheads show the sympathetic chain and dorsal root ganglion (DRG), respectively. (b) BaseScope ISH with *Pcgf1* probe and HuC/D immunostaining of the myenteric plexus from the proximal colon of 3-week-old WT and *Pcgf1*$^{fl/fl}$; *Phox2b*$^{Cre/+}$ mice. Maximum-intensity images were obtained with ImageJ. Scale bars: 50 μm.
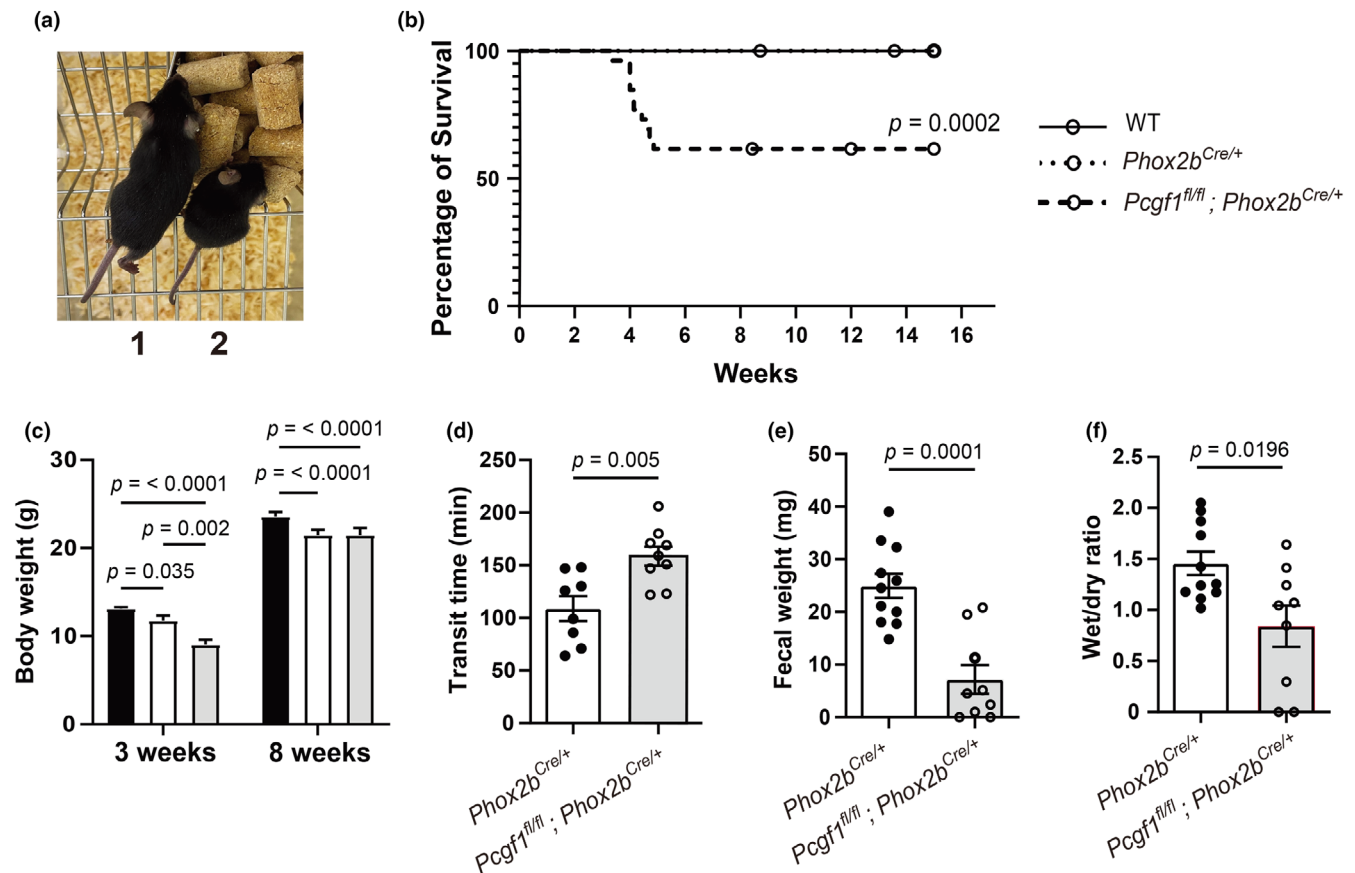
FIGURE 2 *Pcgf1* cKO mice exhibit growth arrest and lower gut motility. (a) *Phox2b$^{Cre/+}$* (1), and (2) *Pcgf1$^{fl/fl}$*; *Phox2b$^{Cre/+}$* mice (2) at 3 weeks of age. (b) Survival analysis between WT ($n = 20$), *Phox2b$^{Cre/+}$* ($n = 29$), and *Pcgf1$^{fl/fl}$*; *Phox2b$^{Cre/+}$* mice ($n = 26$). (c) Body weight comparisons between WT (black bar, $n = 20$), *Phox2b$^{Cre/+}$* (white bar, $n = 26$), and *Pcgf1$^{fl/fl}$*; *Phox2b$^{Cre/+}$* mice (gray bar, $n = 13$) at 3 and 8 weeks of age. (d) Total gastrointestinal transit time (GITT) analysis between 3-week-old *Phox2b$^{Cre/+}$* ($n = 8$) and *Pcgf1$^{fl/fl}$*; *Phox2b$^{Cre/+}$* mice ($n = 9$). (e) Fecal weight comparisons between 3-week-old *Phox2b$^{Cre/+}$* ($n = 8$) and *Pcgf1$^{fl/fl}$*; *Phox2b$^{Cre/+}$* mice ($n = 6$). (f) Fecal water contents between 3-week-old *Phox2b$^{Cre/+}$* ($n = 8$) and *Pcgf1$^{fl/fl}$*; *Phox2b$^{Cre/+}$* ($n = 6$). Survival analysis was conducted using a log-rank test and shown by the Kaplan–Meier graph. Results of statistical analysis are shown as the mean ± SEM using an unpaired *t*-test with Welch's correction.

survival rates (Figure 2b), we observed slight growth retardation in *Phox2b$^{Cre/+}$* mice compared with WT at 3 ($p = 0.035$) and 8 weeks ($p \leq 0.0001$) (Figure 2c). This observation led us to use *Phox2b$^{Cre/+}$* as the control for the following experiments. *Pcgf1$^{fl/fl}$*; *Phox2b$^{Cre/+}$* mice displayed significantly lower body weight than *Phox2b$^{Cre/+}$* mice at 3 weeks ($p = 0.002$), although they could finally catch up with *Phox2b$^{Cre/+}$* mice's growth at 8 weeks (Figure 2c). Only half of *Pcgf1$^{fl/fl}$*; *Phox2b$^{Cre/+}$* mice ($p = 0.0002$) survived to adulthood (Figure 2b). These data suggest that the absence of PCGF1 impacts growth and survival rate.

Macroscopic examination of the gut showed no difference between 3-week-old *Phox2b$^{Cre/+}$* and *Pcgf1$^{fl/fl}$*; *Phox2b$^{Cre/+}$* mice, including gut length (data not shown). Furthermore, we evaluated the effect of *Pcgf1* deletion on gut functions, such as motility and water secretion. GITT was significantly longer in the *Pcgf1$^{fl/fl}$*; *Phox2b$^{Cre/+}$* than *Phox2b$^{Cre/+}$* mice ($p = 0.005$) (Figure 2d). Slower transit was associated with lighter fecal weights ($p = 0.0395$) (Figure 2e) and drier feces in *Pcgf1$^{fl/fl}$*; *Phox2b$^{Cre/+}$* mice ($p = 0.0271$) (Figure 2f). These observations indicate that the absence of PCGF1 impairs gut motility at the early postnatal stage.

Impaired gut motility in *Pcgf1$^{fl/fl}$*; *Phox2b$^{Cre/+}$* mice suggested the presence of anatomical deficits of the ENS. Therefore, we analyzed ENS development and differentiation from embryonic to postnatal stages. The basic structure of the ENS is formed by colonization of the entire gut by migrating ENS precursors, a process is known to occur from E9 to E14 (Obermayr et al., 2013). Examination of the embryonic gut at E14.5 revealed that ENS precursors fully colonized the colon in *Phox2b$^{Cre/+}$* and *Pcgf1$^{fl/fl}$*; *Phox2b$^{Cre/+}$* mice. Moreover, the numbers of ENS precursors, revealed by Phox2B staining, were comparable in these mice. These data suggest that *Pcgf1* deficiency does not influence migration and proliferation of ENS precursors (Figure S2a,b). In newborn mice (P0), the numbers of myenteric neurons in the lower small intestine (LSI: ileum) and colon were comparable between *Phox2b$^{Cre/+}$* and *Pcgf1$^{fl/fl}$*; *Phox2b$^{Cre/+}$* mice (Figure S2c,d). These results suggest that PCGF1 deficiency does not impact ENS development before birth.

At a postnatal stage (3 weeks old), we examined the total numbers of neurons and several neuronal subtypes in the myenteric and submucosal plexus of the *Phox2b$^{Cre/+}$* and *Pcgf1$^{fl/fl}$*; *Phox2b$^{Cre/+}$* mice. The staining of myenteric neurons with HuC/D, a pan-neuronal
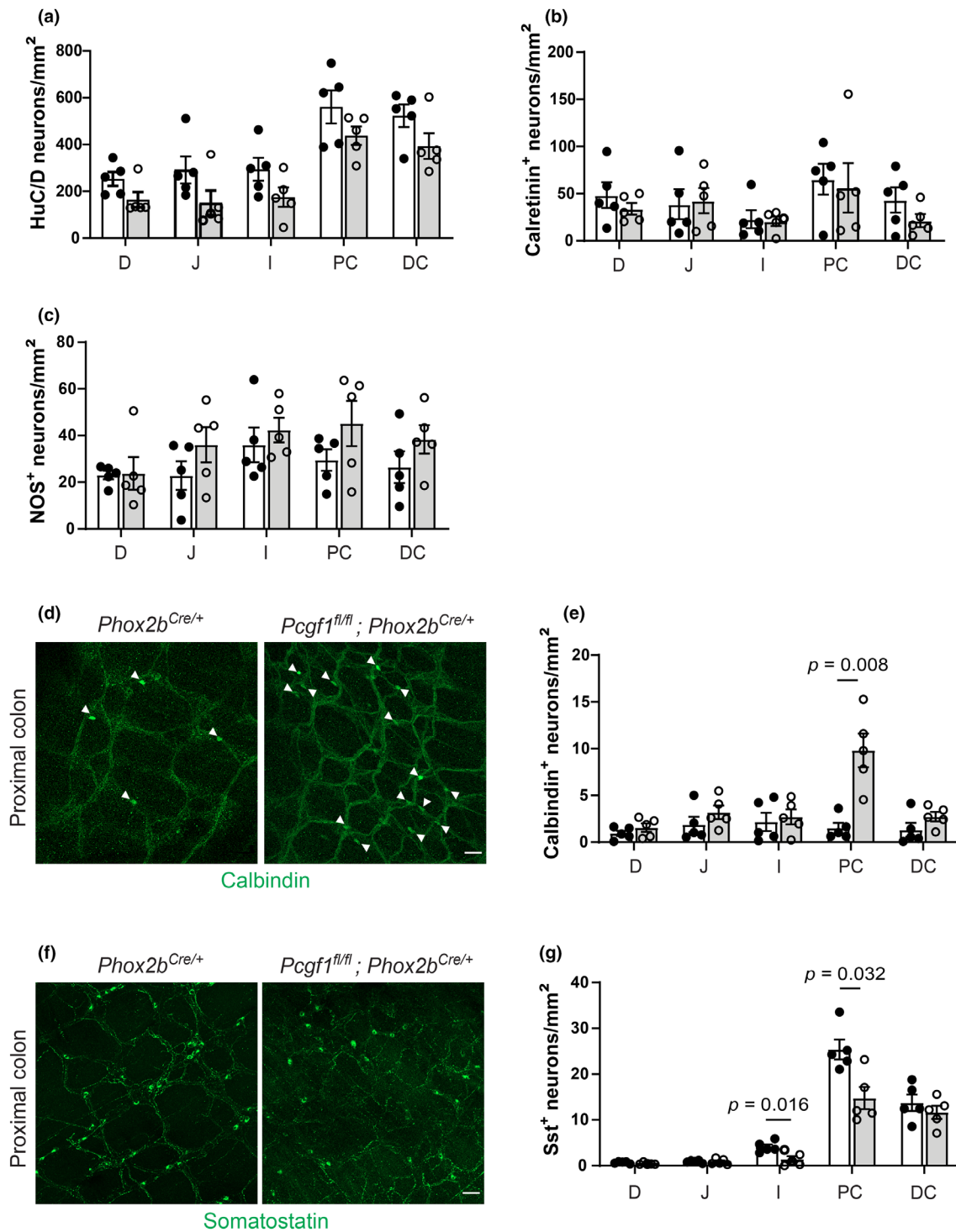
FIGURE 3 *Pcgf1* is involved in specification of enteric neuron subtypes in the myenteric plexus. (a–c) Quantitative analysis of HuC/D (a), calretinin[+] (b), and NOS1^{+} (c) myenteric neurons between 3-week-old *Phox2b*[Cre/+] and *Pcgf1*^{fl/fl}; *Phox2b*[Cre/+] mice ($n = 5$ for each mice group). (d, e) Representative images (d) and quantitative analysis (e) of calbindin[+] myenteric plexus neuron numbers from the 3-week-old *Phox2b*[Cre/+] and *Pcgf1*^{fl/fl}; *Phox2b*[Cre/+] mice ($n = 5$ for each mice group). (f, g) Representative images (f) and quantitative analysis (g) of Sst^{+} myenteric neurons from the 3-week-old *Phox2b*[Cre/+] and *Pcgf1*^{fl/fl}; *Phox2b*[Cre/+] mice ($n = 5$ for each mice group). Quantitative data shown in white bars as *Phox2b*[Cre/+] and gray bars as *Pcgf1*^{fl/fl}; *Phox2b*[Cre/+] mice. D, duodenum; DC, distal colon; I, ileum; J, jejunum; PC, proximal colon. Results of statistical analysis are shown as the mean ± SEM using the Mann–Whitney *U* test. Maximum-intensity images were obtained with ImageJ. Scale bars: 50 μm.
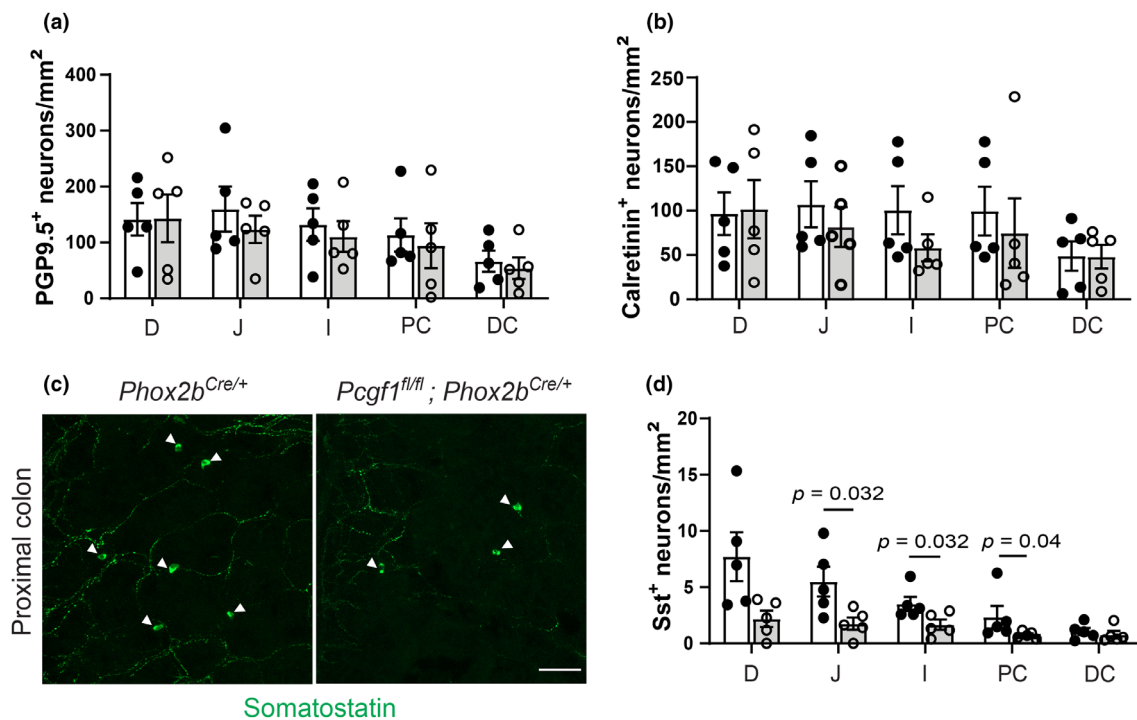
FIGURE 4 The role of *Pcgf1* in the submucosal plexus. (a, b) Quantitative analysis of PGP9.5$^+$ (a) and calretinin$^+$ (b) submucosal neurons between 3-week-old *Phox2b*$^{Cre/+}$ and *Pcgf1*$^{fl/fl}$; *Phox2b*$^{Cre/+}$ mice ($n = 5$ for each mice group). (c, d) Representative images (c) and quantitative analysis (d) of Sst$^+$ neurons from the 3-week-old *Phox2b*$^{Cre/+}$ and *Pcgf1*$^{fl/fl}$; *Phox2b*$^{Cre/+}$ mice ($n = 5$ for each mice group). Quantitative data shown in white bars as *Phox2b*$^{Cre/+}$ and gray bars as *Pcgf1*$^{fl/fl}$; *Phox2b*$^{Cre/+}$. D, duodenum; DC, distal colon; I, ileum; J, jejunum; PC, proximal colon. Results of statistical analysis are shown as the mean ± SEM using the Mann–Whitney *U* test. Maximum-intensity images were obtained with ImageJ. Scale bar: 50 μm.

marker, showed no difference in all gut regions (Figures 3a and S2e). Examination of calretinin- and NOS1-expressing neurons, two major neuronal subtypes, also revealed no significant difference between *Pcgf1*$^{fl/fl}$; *Phox2b*$^{Cre/+}$ and *Phox2b*$^{Cre/+}$ mice (Figure 3b,c). However, we found that the numbers of somatostatin-expressing (Sst$^+$) neurons (descending/inhibitory neurons) were significantly decreased in the ileum ($p = 0.016$) and proximal colon ($p = 0.032$) of *Pcgf1*$^{fl/fl}$; *Phox2b*$^{Cre/+}$ mice as compared with *Phox2b*$^{Cre/+}$ mice (Figure 3f,g). In contrast, the numbers of calbindin$^+$ neurons (ascending/excitatory neurons) were increased ($p = 0.008$) in the proximal colon of *Pcgf1*$^{fl/fl}$; *Phox2b*$^{Cre/+}$ mice (Figure 3d,e). These findings reveal the opposing effects of PCGF1 in determining the numbers of Sst$^+$ and calbindin$^+$ neurons.

Examination of the total numbers of neurons in the submucosal plexus with pan-neuronal marker PGP9.5$^+$ revealed no significant difference in all gut regions between *Pcgf1*$^{fl/fl}$; *Phox2b*$^{Cre/+}$ and *Phox2b*$^{Cre/+}$ mice (Figures 4a and S2f). Although we did not observe the difference in the calretinin$^+$ neurons (Figure 4b), we detected a significant decrease in the numbers of Sst$^+$ neurons in the jejunum ($p = 0.032$), ileum ($p = 0.032$), and proximal colon ($p = 0.04$) in *Pcgf1*$^{fl/fl}$; *Phox2b*$^{Cre/+}$ mice (Figure 4c,d). These analyses reveal that the Sst$^+$ neurons are commonly affected by *Pcgf1* ablation in both the myenteric and submucosal plexus. Taken together, these data suggest that PCGF1 plays a crucial role in neuronal subtype specification in the ENS, especially Sst$^+$ and calbindin$^+$ neuron determinations, without affecting the total neuronal numbers.

4 | DISCUSSION

In this study, we investigated the biological role of PCGF1 in ENS development and maturation. PCGF1 deletion did not affect the basic formation of the ENS, including gut colonization by ENS precursors and total neuron numbers, suggesting that PCGF1 is dispensable for ENS precursor migration and enteric neurogenesis. In this respect, our study suggests that PCGF1 alone is not responsible for the *rnf2*-(PRC1) (Feng & Sun, 2022) or *Aebp2/Ezh2*- (PRC2) (Kim et al., 2011, 2018) deficient phenotypes whose disruption impairs ENS precursor migration and enteric ganglion formation, respectively. *Pcgf1* deficiency specifically impaired Sst$^+$ neuron numbers in the multiple gut regions. Importantly, decreased Sst$^+$ neuron numbers were associated with increased calbindin$^+$ neuron numbers in the proximal colon. The numbers of Sst$^+$ neurons lost were comparable to gained calbindin$^+$ neurons, resulting in similar total numbers between Sst$^+$ and calbindin$^+$ neurons in the control and *Pcgf1*-deficient proximal colon (Figure 3d–g). These findings suggest that excessive calbindin$^+$ neurons are generated at the expense of Sst$^+$ neurons by the loss of *Pcgf1*. Although several studies have shown the involvement of transcription factors, such as *Pbx3*, *Sox6*, and *Tbx3*, in the development of specific neurons in the ENS (Memic et al., 2018; Morarach et al., 2021; Wright et al., 2021), this study provides evidence, for the first time to our knowledge, that epigenetic mechanisms also regulate neuronal subtype specification.

Based on a recently proposed model for subtype specification of enteric neurons in the small intestine (Morarach et al., 2021), PCGF1 may potentially be involved in two differentiation processes. Immature enteric neuron progenitors first differentiate into two branches, one of which (Branch A) further differentiates into five (enteric neuron class [ENC] 8–12) and the other (Branch B) into seven subtypes (ENC1–7). Sst$^+$ neurons belong exclusively to ENC5 (Branch B derivative), whereas most calbindin$^+$ neurons belong to ENC12 (Branch A derivative). This suggests that, if subtype conversion occurs between Branch A and B, PCGF1 should be operational at the bifurcation point and prevent immature neuron progenitors from adopting Branch A's fate (Model A: Figure S3).

Another differentiation process in which PCGF1 is potentially involved is found within Branch B. A small population of calbindin$^+$ neurons belong to ENC7, which differentiates from ENC5 (Sst$^+$). In this transition, PCGF1 may directly suppress the calbindin locus in ENC5 to prevent them from adopting the ENC7 fate. Consistent with this hypothesis, potential *Pcgf1* binding sites, along with H3K27me3 and H2AK119ub1 histones, were found in the *Calb1* locus of the mouse embryonic stem cells via a ChIP-Atlas (http://chip-atlas.org/) (Oki et al., 2018), an open-access chromatin immunoprecipitation sequencing (ChIP-seq) database. PCGF1 could be involved in specification of calbindin$^+$ neurons by its gene repression function during the early developmental stage, which is maintained by H3K27me3 and H2AK119ub1 (Chen et al., 2021). Interestingly, in addition to the proximal colon, decreased Sst$^+$ neurons were found in various gut regions in *Pcgf1*-deficient enteric neuronal lineage. These findings suggest that PCGF1 is generally required for ENC5 to prevent their further differentiation (Model B: Figure S3).

Although our study provides novel insight into the mechanism underlying neuronal subtype specification, several unresolved issues exist. For instance, *Pcgf1$^{fl/fl}$*; *Phox2b$^{Cre/+}$* mice displayed increased lethality, transient growth deficit, and impaired gut function. Although the exact causes of these phenotypes remain elusive, impaired neuronal differentiation may affect gut motility (Sunardi et al., 2022). For instance, we detected increased calbindin$^+$ neurons (ascending/excitatory neurons) and decreased Sst$^+$ (descending/inhibitory neurons) in *Pcgf1$^{fl/fl}$*; *Phox2b$^{Cre/+}$* mice. Such unbalanced excitatory/inhibitory innervation could lead to delayed GITT. In *Pcgf1$^{fl/fl}$*; *Phox2b$^{Cre/+}$* mice, *Pcgf1* gene is disrupted not only in the ENS, but also in the sympathetic and parasympathetic ganglia. We speculate that the *Pcgf1* disruption in those ganglia can impair visceral function and cause lethality. Further studies will be required to address these issues.

AUTHOR CONTRIBUTIONS

Bayu Pratama Putra: Investigation; formal analysis; visualization; writing—original draft. Keisuke Ito: Methodology; investigation; writing—original draft. Carla Cirillo: Investigation; writing–review and editing; Mukhamad Sunardi: Methodology. Haruhiko Koseki: Resources. Toshihiro Uesaka: Methodology; supervision; writing—review and editing. Hideki Enomoto: Conceptualization; supervision; funding acquisition; validation; project administration; writing—original draft, review and editing.

CONFLICT OF INTEREST STATEMENT

The authors have no competing interests to disclose.

ORCID

Hideki Enomoto https://orcid.org/0000-0002-8004-8885

REFERENCES

Almeida, M., Pintacuda, G., Masui, O., Koseki, Y., Gdula, M., Cerase, A., & Brockdorff, N. (2017). PCGF3/5-PRC1 initiates Polycomb recruitment in X chromosome inactivation. *Science*, *356*(6342), 1081–1084. https://doi.org/10.1126/science.aal2512

Aranda, S., Mas, G., & Di Croce, L. (2015). Regulation of gene transcription by Polycomb proteins. *Science Advances*, *1*(11), e1500737. https://doi.org/10.1126/sciadv.1500737

Avetisyan, M., Schill, E. M., & Heuckeroth, R. O. (2015). Building a second brain in the bowel. *Journal of Clinical Investigation*, *125*, 899–907. https://doi.org/10.1172/JCI76307

Bergner, A. J., Stamp, L. A., Gonsalvez, D. G., Allison, M. B., Olson, D. P., Myers, M. G., & Young, H. M. (2014). Birthdating of myenteric neuron subtypes in the small intestine of the mouse. *Journal of Comparative Neurology*, *522*(3), 514–527. https://doi.org/10.1002/cne.23423

Blackledge, N. P., Farcas, A. M., Kondo, T., King, H. W., McGouran, J. F., Hanssen, L. L. P., & Klose, R. J. (2014). Variant PRC1 complex-dependent H2A ubiquitylation drives PRC2 recruitment and polycomb domain formation. *Cell*, *157*(6), 1445–1459. https://doi.org/10.1016/j.cell.2014.05.004

Chalazonitis, A., Pham, T. D., Rothman, T. P., Distefano, P. S., Bothwell, M., Blair-Flynn, J., & Gershon, M. D. (2001). Neurotrophin-3 is required for the survival-differentiation of subsets of developing enteric neurons. *The Journal of Neuroscience*, *21*(15), 5620–5636. https://doi.org/10.1523/JNEUROSCI.21-15-05620.2001

Chen, Z., Djekidel, M. N., & Zhang, Y. (2021). Distinct dynamics and functions of H2AK119ub1 and H3K27me3 in mouse preimplantation embryos. *Nature Genetics*, *53*(4), 551–563. https://doi.org/10.1038/s41588-021-00821-2

Feng, G., & Sun, Y. (2022). The Polycomb group gene rnf2 is essential for central and enteric neural system development in zebrafish. *Frontiers in Neuroscience*, *16*, 960149. https://doi.org/10.3389/fnins.2022.960149

Fukuda, T., Tokunaga, A., Sakamoto, R., & Yoshida, N. (2011). Fbxl10/Kdm2b deficiency accelerates neural progenitor cell death and leads to exencephaly. *Molecular and Cellular Neuroscience*, *46*(3), 614–624. https://doi.org/10.1016/j.mcn.2011.01.001

Fursova, N. A., Blackledge, N. P., Nakayama, M., Ito, S., Koseki, Y., Farcas, A. M., & Klose, R. J. (2019). Synergy between variant PRC1 complexes defines Polycomb-mediated gene repression. *Molecular Cell*, *74*(5), 1020–1036.e8. https://doi.org/10.1016/j.molcel.2019.03.024

Hao, M. M., Foong, J. P. P., Bornstein, J. C., Li, Z. L., Vanden Berghe, P., & Boesmans, W. (2016). Enteric nervous system assembly: Functional integration within the developing gut. *Developmental Biology*, *417*, 168–181. https://doi.org/10.1016/j.ydbio.2016.05.030

Hao, M. M., & Young, H. M. (2009). Development of enteric neuron diversity. *Journal of Cellular and Molecular Medicine*, *13*(7), 1193–1210. https://doi.org/10.1111/j.1582-4934.2009.00813.x

Ikawa, T., Masuda, K., Endo, T. A., Endo, M., Isono, K., Koseki, Y., & Kawamoto, H. (2016). Conversion of T cells to B cells by inactivation

of polycomb-mediated epigenetic suppression of the B-lineage program. *Genes and Development*, 30(22), 2475–2485. https://doi.org/10.1101/gad.290593.116

Kilkenny, C., Browne, W. J., Cuthill, I. C., Emerson, M., & Altman, D. G. (2010). Improving bioscience research reporting: The arrive guidelines for reporting animal research. *PLoS Biology*, 8(6), e1000412. https://doi.org/10.1371/journal.pbio.1000412

Kim, H., Kang, K., Ekram, M. B., Roh, T. Y., & Kim, J. (2011). Aebp2 as an epigenetic regulator for neural crest cells. *PLoS One*, 6(9), e25174. https://doi.org/10.1371/journal.pone.0025174

Kim, H., Langohr, I. M., Faisal, M., McNulty, M., Thorn, C., & Kim, J. (2018). Ablation of Ezh2 in neural crest cells leads to aberrant enteric nervous system development in mice. *PLoS One*, 13(8), e0203391. https://doi.org/10.1371/journal.pone.0203391

Li, X., Ji, G., Zhou, J., Du, J., Li, X., Shi, W., & Hao, A. (2021). Pcgf1 regulates early neural tube development through histone methylation in zebrafish. *Frontiers in Cell and Developmental Biology*, 8, 581636. https://doi.org/10.3389/fcell.2020.581636

Memic, F., Knoflach, V., Morarach, K., Sadler, R., Laranjeira, C., Hjerling-Leffler, J., & Marklund, U. (2018). Transcription and signaling regulators in developing neuronal subtypes of mouse and human enteric nervous system. *Gastroenterology*, 154(3), 624–636. https://doi.org/10.1053/j.gastro.2017.10.005

Molyneaux, B. J., Arlotta, P., Menezes, J. R. L., & Macklis, J. D. (2007). Neuronal subtype specification in the cerebral cortex. *Nature Reviews Neuroscience*, 8, 427–437. https://doi.org/10.1038/nrn2151

Morarach, K., Mikhailova, A., Knoflach, V., Memic, F., Kumar, R., Li, W., Ernfors, P., & Marklund, U. (2021). Diversification of molecularly defined myenteric neuron classes revealed by single-cell RNA sequencing. *Nature Neuroscience*, 24(1), 34–46. https://doi.org/10.1038/s41593-020-00736-x

Nunes, M., Blanc, I., Maes, J., Fellous, M., Robert, B., & McElreavey, K. (2001). NSPc1, a novel mammalian Polycomb gene, is expressed in neural crest-derived structures of the peripheral nervous system. *Mechanisms of Development*, 102(1–2), 219–222. https://doi.org/10.1016/S0925-4773(01)00288-X

Obermayr, F., Hotta, R., Enomoto, H., & Young, H. M. (2013). Development and developmental disorders of the enteric nervous system. *Nature Reviews Gastroenterology and Hepatology*, 10, 43–57. https://doi.org/10.1038/nrgastro.2012.234

Oki, S., Ohta, T., Shioi, G., Hatanaka, H., Ogasawara, O., Okuda, Y., & Meno, C. (2018). Ch IP-atlas: A data-mining suite powered by full integration of public Ch IP-seq data. *EMBO Reports*, 19(12), e46255. https://doi.org/10.15252/embr.201846255

Schneider, C. A., Rasband, W. S., & Eliceiri, K. W. (2012). NIH image to ImageJ: 25 years of image analysis. *Nature Methods*, 9, 671–675. https://doi.org/10.1038/nmeth.2089

Sugishita, H., Kondo, T., Ito, S., Nakayama, M., Yakushiji-Kaminatsui, N., Kawakami, E., Koseki, Y., Ohinata, Y., Sharif, J., Harachi, M.,

Blackledge, N. P., Klose, R. J., & Koseki, H. (2021). Variant PCGF1-PRC1 links PRC2 recruitment with differentiation-associated transcriptional inactivation at target genes. *Nature Communications*, 12(1), 5341. https://doi.org/10.1038/s41467-021-24894-z

Sunardi, M., Ito, K., Sato, Y., Uesaka, T., Iwasaki, M., & Enomoto, H. (2022). A single RET mutation in Hirschsprung disease induces intestinal Aganglionosis via a dominant-negative mechanism. *Cellular and Molecular Gastroenterology and Hepatology*, 15, 1505–1524. https://doi.org/10.1016/j.jcmgh.2022.12.003

Vicentini, F. A., Keenan, C. M., Wallace, L. E., Woods, C., Cavin, J. B., Flockton, A. R., & Sharkey, K. A. (2021). Intestinal microbiota shapes gut physiology and regulates enteric neurons and glia. *Microbiome*, 9(1), 210. https://doi.org/10.1186/s40168-021-01165-z

Vohra, B. P. S., Tsuji, K., Nagashimada, M., Uesaka, T., Wind, D., Fu, M., & Heuckeroth, R. O. (2006). Differential gene expression and functional analysis implicate novel mechanisms in enteric nervous system precursor migration and neuritogenesis. *Developmental Biology*, 298(1), 259–271. https://doi.org/10.1016/j.ydbio.2006.06.033

Wright, C. M., Schneider, S., Smith-Edwards, K. M., Mafra, F., Leembruggen, A. J. L., Gonzalez, M. V., & Heuckeroth, R. O. (2021). scRNA-seq reveals new enteric nervous system roles for GDNF, NRTN, and TBX3. *Cellular and Molecular Gastroenterology and Hepatology*, 11(5), 1548–1592.e1. https://doi.org/10.1016/j.jcmgh.2020.12.014

Yan, Y., Zhao, W., Huang, Y., Tong, H., Xia, Y., Jiang, Q., & Qin, J. (2017). Loss of Polycomb group protein Pcgf1 severely compromises proper differentiation of embryonic stem cells. *Scientific Reports*, 7, 46276. https://doi.org/10.1038/srep46276

Yoshioka, Y., Tachibana, Y., Uesaka, T., Hioki, H., Sato, Y., Fukumoto, T., & Enomoto, H. (2022). Uts2b is a microbiota-regulated gene expressed in vagal afferent neurons connected to enteroendocrine cells producing cholecystokinin. *Biochemical and Biophysical Research Communications*, 608, 66–72. https://doi.org/10.1016/j.bbrc.2022.03.117

SUPPORTING INFORMATION

Additional supporting information can be found online in the Supporting Information section at the end of this article.